Analytical Examination on the Amplifying Effect of Weak Grid Connection for the DFIGs to Induce Torsional Sub-synchronous Oscillations

Wenjuan Du, *Member, IEEE*, Yang Wang, Haifeng Wang, *Senior Member, IEEE*, Xianyong Xiao, Xubin Wang, and Xiaorong Xie

***Abstract*—This paper analytically examines how the condition of weak grid connection affects the torsional sub-synchronous oscillations (SSOs) induced by a grid-connected DFIG in a power system. The examination focuses on the SSO mode of grid-connected DFIG, which is dominated by the phase locked loop (PLL) or DC voltage control. Theoretical analysis is carried out to prove that the condition of weak grid connection amplifies the impact of modal resonance between the DFIG and torsional dynamics of synchronous generators. The amplifying effect of weak grid connection exhibits as the decrease of damping of SSO mode of DFIG and increase of the associated residue when the grid connection weakens. Consequently, the DFIG is more likely to induce torsional SSOs under the condition of weak grid connection, leading to system instability in the worst case. Analytical examination presented in the paper reveals the mechanism about how the condition of weak grid connection plays a key role for the DFIG to induce the torsional SSOs. An example multi-machine power system with the grid-connected DFIG is presented. Results of modal analysis and non-linear simulation using detailed model of DFIG validate the analysis and conclusions made in the paper.**

***Index Terms*—Sub-synchronous oscillations, grid-connected DFIG, torsional dynamics of synchronous generators, weak grid connection.**

I. Introduction

A. Literature Review and Motivation of the Paper

IT HAS been recognized for long time that a grid-connected VSC based system, such as the DFIG for the wind power generation, may suffer the problem of small-signal instability under the condition of weak grid connection. The instability danger was closely related with the dynamics of the PLL or DC voltage control. Modal analysis found that when the grid connection becomes weaker, the oscillation modes of grid-connected VSC based system, dominated by the PLL or DC voltage control, moved towards the right on the complex plane, leading to growing oscillations in the worst case [1]–[7].

Recognition about the condition of weak grid connection outlined above was established mainly on the basis of numerical evaluation of examples with detailed model of VSC based systems being used. In order to gain better understanding on and deeper insight into the instability mechanism, theoretical analysis about the destabilizing effect of weak grid connection of wind turbine generators (WTGs) was presented in [8]–[10]. Under the assumptions to simplify the model of a grid-connected VSC, it was proved in [8] that condition of weak grid connection amplified the modal resonance between the PLL and DC voltage control to lead to growing oscillations. Simplified models of type 4 WTG were evaluated in details in [9] and compared with the detailed model. The instability danger was analytically attributed to a zero of type 4 WTG on the right half of complex plane [10]. Recent study in [8]–[10] demonstrated the necessity and benefit of theoretical analysis based on the simplified models of grid-connected WTGs. This has motivated the work presented in this paper.

The second motivation of the work presented in the paper is the recently reported incidents of sub-synchronous oscillations (SSOs) caused by grid-connected WTGs in the Harmi area in the western power system of China. At least in one reported incident, the torsional dynamics of synchronous generators (SGs) in the power system were excited, which has caused great concerns [11]–[13]. It was suspected that the condition of weak grid connection may have played certain role for the WTGs to induce the SSOs, because the majority of wind farms in the Harmi area were weakly connected to the main grid via long transmission lines.

On the other hand, modal resonance analysis conducted in [12], [13] explained why the torsional SSO mode of the SG may be "excited" by grid-connected WTGs to cause growing torsional SSOs in a power system. The analysis revealed the mechanism of "excitation". However, the role played by the condition of weak grid connection was completely missed out

Manuscript received July 5, 2019; revised October 3, 2019; accepted November 16, 2019. Date of publication December 2, 2019; date of current version July 23, 2020. This work was supported by the State Grid Corporation of China (Oscillation risk analysis and simulation technology research of wind power generator groups and flexible HVDC interconnection system), under Grant NYB17201800102. Paper no. TPWRD-00731-2019. *(Corresponding authors: Yang Wang and Haifeng Wang.)*

W. Du, H. Wang, and X. Xiao are with the School of Electrical Engineering, Sichuan University, Chengdu 610065, China (e-mail: ddwenjuan@qq.com; hfwang60@qq.com; xiaoxianyong@163.com).

Y. Wang is with the State Key Laboratory of Alternate Electric Power Systems with New Energy Resources, North China Electric Power University, Beijing 102206, China (e-mail: wangyang_ncepu@126.com).

X. Wang is with the State Grid Energy Research Institute Co., LTD., Beijing 102209, China (e-mail: wbin.great@gmail.com).

X. Xie is with the Department of Electrical Engineering, Tsinghua University, Beijing 100084, China (e-mail: xiexr@tsinghua.edu.cn).

Color versions of one or more of the figures in this article are available online at http://ieeexplore.ieee.org.

Digital Object Identifier 10.1109/TPWRD.2019.2957005

in [12], [13]. Hence, the mechanism that the WTGs "excite" the torsional SSOs under the condition of weak grid connection has remained unknown. Revelation of the mechanism is important for investigating and understanding the SSO incidents in the Harmi power system in the western China.

B. Strategy of Investigation Adopted and Contributions Made in the Paper

This paper analytically investigates how the weak grid connection of a DFIG may affect its modal resonance with the torsional dynamics of the SGs. The purpose of investigation is to fill in the gaps of study outlined above by revealing the role played by the condition of weak grid connection in the mechanism that the DFIG excites the torsional SSOs. The strategy of investigation adopted in the paper is as follows.

First, the investigation is based on the theory of modal resonance when an oscillation mode of the DFIG is coupled with a torsional SSO mode of the SG [12], [13]. Focus of investigation in the paper is on the following two types of oscillation modes of the DFIG: (1) The oscillation mode associated with the PLL. (2) The oscillation mode related with the DC voltage control. This is because frequency of those two types of oscillation modes is normally in the range of frequency of torsional SSOs [3]–[7]. In addition, under the condition of weak grid connection, those two types of oscillation modes more likely become poorly damped [3]–[7].

Second, study cases reported in the literature so far have indicated that when the grid connection of the DFIG becomes weaker, damping of the oscillation mode associated with either the PLL [3]–[5] or the DC voltage control [6]–[7] decreases. Hence, in the timescale of dynamics of either the PLL or the DC voltage control, poorly damped oscillation mode associated with either the PLL or the DC voltage control is the dominant conjugate pole of the DFIG. Even in the case that dynamics of the PLL and DC voltage control are coupled due to the modal resonance, only one of two oscillation modes associated with the PLL and DC voltage control may become poorly damped [8] and hence is the dominant conjugate pole of the DFIG.

Third, according to control system theory, if dynamics of a control system are dominated by a conjugate pole, full-order model of the control system can be simplified to a second-order system with the conjugate pole only and other dynamics being neglected [14]. Dynamics of the simplified second-order system can approximately represent the dynamics of the full-order system [14].

Therefore, this paper considers the cases that two types of oscillation modes of the DFIG associated with the PLL or the DC voltage control are the dominant conjugate poles of the DFIGs separately. Based on the consideration, simplified model of the DFIG dominated by either the PLL or the DC voltage control is derived. The simplified model makes it possible to analytically examine how the condition of weak grid connection may affect the modal resonance between the DFIG and torsional dynamics of the SG with the following conclusions theoretically proved: When the condition of grid connection weakens, damping of SSO mode of the DFIG decreases and the residue associated with the SSO mode increases. This implies that the weak grid connection amplifies the impact of modal resonance. Consequently, under the condition of weak grid connection, the DFIG is more likely to induce growing torsional SSOs when the modal resonance happens. Hence, main contributions of the paper are summarized as follows.

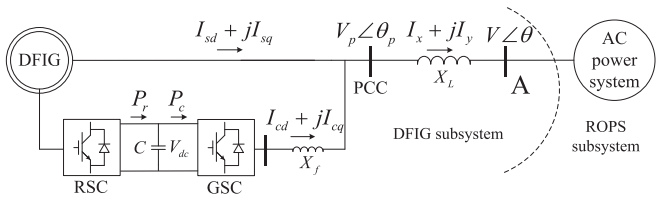

Fig. 1. A DFIG connected to an external AC power system.

Analytical examination reveals the amplifying effect of weak grid connection for the DFIG to excite the torsional SSO mode of synchronous generators. This is the further advance of study on the subject from the work presented in [8]–[11] and [12]–[13]. This helps considerably to understand the mechanism of SSO incidents in Harmi power system.

II. Analytical Examination

A. Condition of Weak Grid Connection and Review of Modal Resonance Theory

Fig. 1 shows a DFIG being connected to an external AC power system via a transmission line, which is represented by a lumped reactance X_L. Dynamics of SGs in the external AC power system are included. Hence, node A is not an infinite AC busbar. Inclusion of SG's dynamics is the main difference of the system being studied in the paper to that previously being examined in [3]–[7]. Condition of grid connection of the DFIG is usually evaluated by the short circuit ratio (SCR), which is defined as [15]

$$SCR = \frac{{V_{p0}}^2}{X_L P_{rated}} \tag{1}$$

where P_{rated} is the rated capacity of the DFIG, V_p is the magnitude of voltage at the point of common coupling (PCC) of the DFIG and subscript 0 refers to the value of a variable at the steady state. If the SCR is smaller than 3, the grid connection of the DFIG is considered being weak [6], [15]. Hence, the bigger X_L or/and P_{rated} are, the weaker the grid connection of the DFIG is. In [5]–[7], the small-signal stability of the grid-connected VSC system as affected by the active power output from the DFIG at the steady state, denoted as P_0 in this paper, was examined and evaluated by study cases. Results of examination indicated that the impact of P_0 was as same as that of X_L. Higher P_0 implies that the grid-connected VSC is of higher rated capacity and hence the SCR is lower. For simplicity of discussion in this paper, X_L and P_0 are considered as two factors to affect the SCR. However, it is worthwhile to point out that the grid strength can often refer to X_L only and P_0 is the steady-state power output from the DFIG [5]–[7].

Modal resonance between the DFIG and SGs was studied in [12] by dividing the power system of Fig. 1 into two subsystems.

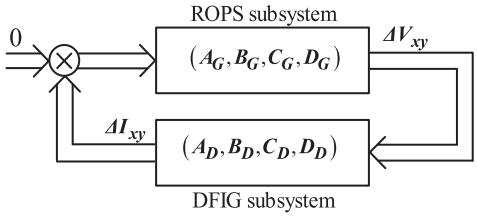

Fig. 2. Interconnected model with division at point A in Fig. 1.

Hence, denote $I_x + jI_y$ as the line current and $V_x + jV_y$ as the voltage at node A, expressed in the common $x-y$ coordinate of the AC power system. The system of Fig. 1 can be divided into two subsystems as shown by Fig. 2. The state-space model of the DFIG subsystem and the subsystem of rest of the power system (ROPS) in Fig. 2 can be written respectively as

$$\text{DFIG subsystem}: \frac{d}{dt}\boldsymbol{\Delta X_D} = \boldsymbol{A_D}\boldsymbol{\Delta X_D} + \boldsymbol{B_D}\boldsymbol{\Delta V_{xy}}$$
$$\boldsymbol{\Delta I_{xy}} = \boldsymbol{C_D}\boldsymbol{\Delta X_D} + \boldsymbol{D_D}\boldsymbol{\Delta V_{xy}} \quad (2)$$

$$\text{ROPS subsystem}: \frac{d}{dt}\boldsymbol{\Delta X_G} = \boldsymbol{A_G}\boldsymbol{\Delta X_G} + \boldsymbol{B_G}\boldsymbol{\Delta I_{xy}}$$
$$\boldsymbol{\Delta V_{xy}} = \boldsymbol{C_G}\boldsymbol{\Delta X_G} + \boldsymbol{D_G}\boldsymbol{\Delta I_{xy}} \quad (3)$$

where prefix Δ denotes the small deviation of a variable or variable vector; $\boldsymbol{\Delta I_{xy}} = [\Delta I_x\ \Delta I_y]^T, \boldsymbol{\Delta V_{xy}} = [\Delta V_x\ \Delta V_y]^T$; $\mathbf{\Delta X_D}$ and $\mathbf{\Delta X_G}$ are respectively the vectors of all the state variables of DFIG subsystem and ROPS subsystem.

Denote λ_d and λ_g respectively as an SSO mode of the DFIG subsystem and the ROPS subsystem. They are the eigenvalues of state matrices, $\mathbf{A_D}$ in (2) and $\mathbf{A_G}$ in (3), respectively. Denote $\mathbf{w_d}^T$ and $\mathbf{v_d}$ as the left and right eigenvectors for λ_d. Denote $\mathbf{w_g}^T$ and $\mathbf{v_g}$ as the left and right eigenvectors for λ_g. Following 2×2 residue matrices for the DFIG and ROPS subsystem can be calculated by using the standard formulas given in [16] as

$$\boldsymbol{R_D} = \boldsymbol{C_D v_d} \times \boldsymbol{w_d}^T \boldsymbol{B_D}, \boldsymbol{R_G} = \boldsymbol{C_G v_g} \times \boldsymbol{w_g}^T \boldsymbol{B_G} \quad (4)$$

Denote the transfer function matrix of the DFIG subsystem and the ROPS subsystem respectively as

$$\mathbf{D}(s) = \begin{bmatrix} d_{11}(s) & d_{12}(s) \\ d_{21}(s) & d_{22}(s) \end{bmatrix}, \mathbf{G}(s) = \begin{bmatrix} g_{11}(s)\ g_{12}(s) \\ g_{21}(s)\ g_{22}(s) \end{bmatrix} \quad (5)$$

The elements in the above open-loop transfer function matrices can be expressed as

$$d_{11}(s) = \frac{R_{D11}}{s-\lambda_d} + \sum_{n=1} \frac{R_{D11n}}{s-\lambda_{dn}} + d_{d11},$$
$$d_{12}(s) = \frac{R_{D12}}{s-\lambda_d} + \sum_{n=1} \frac{R_{D12n}}{s-\lambda_{dn}} + d_{d12},$$
$$d_{21}(s) = \frac{R_{D21}}{s-\lambda_d} + \sum_{n=1} \frac{R_{D21n}}{s-\lambda_{dn}} + d_{d21},$$
$$d_{22}(s) = \frac{R_{D22}}{s-\lambda_d} + \sum_{n=1} \frac{R_{D22n}}{s-\lambda_{dn}} + d_{d22}, \quad (6)$$

$$g_{11}(s) = \frac{R_{G11}}{s-\lambda_g} + \sum_{n=1} \frac{R_{G11n}}{s-\lambda_{gn}} + d_{g11},$$
$$g_{12}(s) = \frac{R_{G12}}{s-\lambda_g} + \sum_{n=1} \frac{R_{G12n}}{s-\lambda_{gn}} + d_{g12},$$
$$g_{21}(s) = \frac{R_{G21}}{s-\lambda_g} + \sum_{n=1} \frac{R_{G21n}}{s-\lambda_{gn}} + d_{g21},$$
$$g_{22}(s) = \frac{R_{G22}}{s-\lambda_g} + \sum_{n=1} \frac{R_{G22n}}{s-\lambda_g} + d_{g22} \quad (7)$$

where $\lambda_{dn}, n = 1, 2, \ldots,$ are the poles of open-loop DFIG subsystem, $R_{Dkmn}, k = 1, 2; m = 1, 2; n = 1, 2, \ldots,$ are the corresponding residues; $R_{Dkm}, k = 1, 2; m = 1, 2,$ are the *k*th-row and *m*th-column elements of residue matrices $\boldsymbol{R_D}$ for λ_d; $\lambda_{gn}, n = 1, 2, \ldots,$ are the poles of open-loop ROPS subsystem, $R_{Gkmn}, k = 1, 2; m = 1, 2; n = 1, 2, \ldots,$ are the corresponding residues; $R_{Gkm}, k = 1, 2; m = 1, 2,$ are the *k*th-row and *m*th-column elements of residue matrices $\boldsymbol{R_G}$ for λ_g.

Modal resonance is the closeness of λ_g and λ_d on the complex plane, i.e., $\lambda_g \approx \lambda_d$ [12]–[13]. Following estimation of the closed-loop SSO modes $\hat{\lambda}_g$ and $\hat{\lambda}_d$ was derived in [12]–[13].

$$\hat{\lambda}_g \approx \lambda_g \pm R_{DG}$$
$$\hat{\lambda}_d \approx \lambda_d \pm R_{DG} \quad (8)$$

where $R_{DG}=\sqrt{R_{D11}R_{G11} + R_{D12}R_{G21} + R_{D21}R_{G12} + R_{D22}R_{G22}}$.

Furthermore, when the modal resonance happens, if

$$|\text{Real part of } R_{DG}| > |\text{Real part of } \lambda_g \approx \lambda_d| \quad (9)$$

the DFIG may very likely induce growing SSOs in the power system.

From (9), it can be seen that if the damping of resonant SSO modes, λ_d and λ_g, is poorer or the residue is bigger, it is more likely that the modal resonance may lead to growing SSOs.

B. SSO mode of DFIG Subsystem Dominated by the PLL

Three main parts in the DFIG subsystem closely related with the condition of grid connection are the converter control systems, the PLL and the transmission line connecting the DFIG to grid. According to the control system theory about the dominant conjugate pole (oscillation mode) [14], when the SSO mode of DFIG subsystem dominated by the PLL under the condition of weak grid connection is examined, the dynamics of converter control systems of the DFIG can be ignored. This simplifies the dynamic model of DFIG subsystem to make theoretical analysis possible. The simplified model contains only dynamics of the PLL. Hence, any SSO mode of simplified model is dominated by the PLL. This is the strategy adopted in the following analytical examination.

First, the synchronous reference frame (SRF) PLL is used as an example in the examination because it is the simplest and most widely applied PLL [17], [18]. Its configuration is shown by Fig. 3 [19], where ω_0 is the synchronous speed, $V_{pd} + jV_{pq}$ is the expression of PCC voltage, $V_p \angle \theta_p$, in the $d-q$ of the DFIG; θ_{pll} is the tracked phase of θ_p by the PLL, which determines the

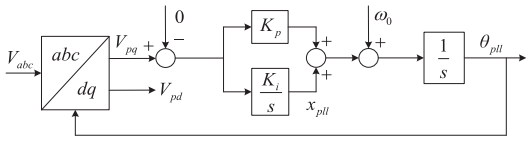

Fig. 3. Configuration of a SRF PLL.

relative position of $d-q$ in respect to $x-y$ coordinate. From Fig. 3, following linearized model of the SRF PLL is obtained

$$\frac{d\Delta\theta_{pll}}{dt} = K_p\Delta V_{pq} + \Delta x_{pll}, \frac{d\Delta x_{pll}}{dt} = K_i\Delta V_{pq} \tag{10}$$

Linearized voltage equations across line, X_L, in Fig. 1 are

$$\Delta V_{px} = \Delta V_x - X_L\Delta I_y, \Delta V_{py} = \Delta V_y + X_L\Delta I_x \tag{11}$$

where $V_{px} + jV_{py}$ is the expression of PCC voltage, $V_p\angle\theta_p$, in the $x-y$ coordinate.

From (10) and (11), the simplified state-space model of the DFIG subsystem described by (2) is derived in Appendix A with

$$\begin{aligned}
\boldsymbol{\Delta X_D} &= \begin{bmatrix}\Delta\theta_{pll} & \Delta x_{pll}\end{bmatrix}^T \\
\boldsymbol{A_D} &= \frac{1}{a}\begin{bmatrix}-(V_{p0}\sqrt{V_{p0}^2V_0^2 - P_0^2X_L^2})K_p & 1\\ -(V_{p0}\sqrt{V_{p0}^2V_0^2 - P_0^2X_L^2})K_i & 0\end{bmatrix} \\
\boldsymbol{B_D} &= \frac{1}{a}\begin{bmatrix}-V_{p0}^2\sin\theta_{p0}K_p & V_{p0}^2\cos\theta_{p0}K_p\\ -V_{p0}^2\sin\theta_{p0}K_i & V_{p0}^2\cos\theta_{p0}K_i\end{bmatrix} = \frac{1}{a}\boldsymbol{B_{pll}} \\
\boldsymbol{C_D} &= \frac{1}{a}\begin{bmatrix}-I_{y0} - bV_{p0}\cos\theta_{p0} & \\ -bX_L(I_{q0}\cos\theta_{p0} + I_{y0}) & 0\\ I_{x0} - bV_{p0}\sin\theta_{p0} & \\ -bX_L(I_{q0}\sin\theta_{p0} - I_{x0}) & 0\end{bmatrix} \\
&= \frac{1}{a}\boldsymbol{C}_{pll} \\
\boldsymbol{D_D} &= \frac{b}{a}\begin{bmatrix}-V_{p0}^2\cos\theta_{p0}\sin\theta_{p0} & V_{p0}^2\cos^2\theta_{p0}\\ V_{p0}^2\sin^2\theta_{p0} & V_{p0}^2\cos\theta_{p0}\sin\theta_{p0}\end{bmatrix}
\end{aligned} \tag{12}$$

where $a=(1-\omega_{r0})\sqrt{V_{p0}^2V_0^2 - P_0^2X_L^2}$, $b=\frac{\omega_{r0}-1}{V_{p0}}I_{sq0} - \frac{\omega_{r0}}{X_{ss}}$. Note that in per unit, $V_{p0}V_0 > P_0X_L$.

Denote $\lambda_{pll} = \xi_{pll} \pm j\omega_{pll}$ as the SSO mode of the DFIG subsystem dominated by the PLL. $\lambda_{pll} = \xi_{pll} \pm j\omega_{pll}$ are the pair of conjugate eigenvalues of $\boldsymbol{A_D}$ in (12). It can have

$$\begin{aligned}
&\xi_{pll} + j\omega_{pll} + \xi_{pll} - j\omega_{pll} = 2\xi_{pll} \\
&= Trace(\boldsymbol{A_D}) = -\frac{\sqrt{V_{p0}^2V_0^2 - P_0^2X_L^2}}{a}V_{p0}K_p
\end{aligned} \tag{13}$$

where $Trace(\boldsymbol{A_D})$ denotes the trace of $\boldsymbol{A_D}$, i.e., the summation of diagonal elements of $\boldsymbol{A_D}$.

From (12),

$$\begin{aligned}
\frac{\partial}{\partial X_L}Trace(\boldsymbol{A_D}) &= \frac{\omega_{r0}V_{p0}^3P_0^2X_L}{a^2\sqrt{V_{p0}^2V_0^2 - P_0^2X_L^2}}K_p > 0 \\
\frac{\partial}{\partial P_0}Trace(\boldsymbol{A_D}) &= \frac{\omega_{r0}V_{p0}^3P_0X_L^2}{a^2\sqrt{V_{p0}^2V_0^2 - P_0^2X_L^2}}K_p > 0
\end{aligned} \tag{14}$$

From (14), it can be concluded that when X_L or/and P_0 increases such that condition of grid connection of the DFIG becomes weaker, real part of SSO mode of the DFIG subsystem dominated by the PLL increases. Subsequently, $\lambda_{pll} = \xi_{pll} \pm j\omega_{pll}$ moves towards the right on the complex plane.

Denote $\lambda_g = \xi_g \pm j\omega_g$ as a torsional SSO mode of the SG, which is an SSO mode of ROPS subsystem in Fig. 2. If $\lambda_g = \xi_g \pm j\omega_g$ is lightly damped [20], $|\xi_g|$ is small such that $\lambda_g \approx j\omega_g$. The conclusion derived above from (14) implies that under the condition of weak grid connection, $|\xi_{pll}|$ becomes small such that $\lambda_{pll} \approx j\omega_{pll}$. Therefore, when the frequencies of $\lambda_g = \xi_g \pm j\omega_g$ and $\lambda_{pll} = \xi_{pll} \pm j\omega_{pll}$ are approximately matched, i.e., $\omega_g \approx \omega_{pll}$, it would have $\lambda_d \approx \lambda_g$. Consequently, the modal resonance happens. In addition, magnitude of real part of resonant SSO modes is small under the condition of weak grid connection such that (9) may more likely stand. Hence, growing SSOs are more possibly induced by the DFIG.

From (4) and (12), the residue matrix of DFIG subsystem can be obtained to be

$$\boldsymbol{R}_D = \frac{1}{a^2}\boldsymbol{C}_{pll}\boldsymbol{v}_p\boldsymbol{w}_p{}^T\boldsymbol{B}_{pll} \tag{15}$$

From (12) and (15), it can be seen that when X_L or/and P_0 increase, a^2 decreases such that the magnitude of $\boldsymbol{R}_D$ increases. Hence, from (9) it can be concluded that under the condition of weaker grid connection, modal resonance between the PLL and the torsional dynamics of the SG is stronger such that growing SSOs are more possibly induced by the DFIG.

C. SSO mode of DFIG Subsystem Dominated by the DC Voltage Control

DC voltage dynamics may bring about instability danger to the single-DFIG infinite-grid system. In this subsection, the case that the DFIG subsystem is dominated by the DC voltage control of the GSC (grid side converter) is examined. For the examination, a simplified state-space model of the DFIG subsystem is derived with only dynamics of the DC voltage control are included. The simplification is made with the consideration that the SSO mode associated with the DC voltage control is the dominant conjugate pole of the DFIG subsystem.

The dynamics of DC voltage control are depicted by the following equations.

$$\begin{cases} CV_{dc0}\frac{d\Delta V_{dc}}{dt} = \Delta P_r - \Delta P_c \\ \frac{d\Delta x_{dc}}{dt} = K_{dci}\Delta V_{dc}\end{cases} \tag{16}$$

where x_{dc} and K_{dci} are the output and gain of integral controller of the DC voltage control of the GSC respectively. When only the dynamics of DC voltage control are considered, the simplified

state-space model of the DFIG subsystem are described by (2) with (see Appendix B for details).

$$\begin{aligned}
\boldsymbol{X_D} &= \begin{bmatrix} \Delta V_{dc} & \Delta x_{dc} \end{bmatrix}^T,\\
\boldsymbol{A_D} &= \begin{bmatrix} -\frac{V_0^2 c - P_0^2 X_L^2}{C V_{dc0} V_0 c} K_{dcp} & -\frac{V_0^2 c - P_0^2 X_L^2}{C V_{dc0} V_0 c} \\ K_{dci} & 0 \end{bmatrix}\\
\boldsymbol{B_D} &= \frac{1}{c}\begin{bmatrix} -P_0 V_{x0} & -P_0 V_{y0} \\ 0 & 0 \end{bmatrix} = \frac{1}{c}\boldsymbol{B_{dc}},\\
\boldsymbol{C_D} &= \frac{1}{c}\begin{bmatrix} c_{11} & c_{12} \\ c_{21} & c_{22} \end{bmatrix} = \frac{1}{c}\boldsymbol{C_{dc}}\\
\boldsymbol{D_D} &= \frac{1}{c}\begin{bmatrix} V_{py0} I_{y0} & -V_{px0} I_{y0} \\ -V_{py0} I_{x0} & V_{px0} I_{x0} \end{bmatrix}
\end{aligned} \tag{17}$$

where K_{dcp} is the proportional gain of the DC voltage controller,

$$\begin{aligned}
c &= \sqrt{V_{p0}^2 V_0^2 - P_0^2 X_L^2}, c_{11}\\
&= (V_{p0}^2 V_{px0} + V_{py0}^2 V_{x0} + V_{px0} V_{py0} V_{y0}) K_{dcp}\\
c_{12} &= V_{p0}^2 V_{px0} + V_{py0}^2 V_{x0} + V_{px0} V_{py0} V_{y0}\\
c_{21} &= (V_{p0}^2 V_{py0} - V_{px}^2 V_{y0} + V_{px0} V_{py0} V_{x0}) K_{dcp}\\
c_{22} &= V_{p0}^2 V_{py0} - V_{px}^2 V_{y0} + V_{px0} V_{py0} V_{x0}
\end{aligned}$$

Denote $\lambda_{dc} = \xi_{dc} \pm j\omega_{dc}$ as the pair of conjugate eigenvalues of state matrix $\boldsymbol{A_D}$ in (17). Obviously, $\lambda_{dc} = \xi_{dc} \pm j\omega_{dc}$ is the SSO mode of the DFIG subsystem dominated the dynamics of DC voltage control of the GSC. From (17),

$$2\xi_{dc} = Trace(\boldsymbol{A_D}) = -\frac{V_0^2 c - P_0^2 X_L^2}{C V_{dc0} V_0 c} K_{dcp} \tag{18}$$

From (18),

$$\begin{aligned}
\frac{\partial}{\partial X_L} Trace(\boldsymbol{A_D}) &= \frac{P_0^2 X_L (2V_{p0}^2 V_0^2 - P_0^2 X_L)}{C V_{dc0} V_{p0} c^3} K_{dcp} > 0\\
\frac{\partial}{\partial P_0} Trace(\boldsymbol{A_D}) &= \frac{P_0 X_L^2 (2V_{p0}^2 V_0^2 - P_0 X_L^2)}{C V_{dc0} V_{p0} c^3} K_{dcp} > 0
\end{aligned} \tag{19}$$

From (4) and (17), residue matrix of DFIG subsystem can be obtained to be

$$\boldsymbol{R}_D = \frac{1}{c^2}\boldsymbol{C}_{dc}\boldsymbol{v}_d{\boldsymbol{w}_d}^T\boldsymbol{B}_{dc} \tag{20}$$

From (19) and (20), it can be concluded that when X_L or/and P_0 increase such that grid connection of the DFIG becomes weaker, the SSO mode of the DFIG subsystem dominated by the DC voltage control moves towards the right on the complex plane. Hence, it is more likely that modal resonance may happen between the DFIG and the torsional dynamics of the SGs when their frequencies are approximately matched. In addition, when the grid connection is weaker, the modal resonance is stronger, because c^2 decreases. Consequently, growing SSOs are more possibly induced by the DFIG.

D. SSO Modes of DFIG Subsystem Dominated by Both the PLL and DC Voltage Control

When the dynamics of both the PLL and DC voltage control described by (10) and (16) are considered, the grid-connected DFIG is dominated by both the PLL and DC voltage control. Following simplified 4th-order state-space model of the DFIG subsystem can be derived (see Appendix C for details of derivation)

$$\boldsymbol{\Delta X_D} = \begin{bmatrix} \Delta\theta_{pll} & \Delta x_{pll} & \Delta V_{dc} & \Delta x_{dc} \end{bmatrix}^T$$

$$\boldsymbol{A_D} = \begin{bmatrix} \frac{-\sqrt{V_{p0}^2 V_0^2 - P_0^2 X_L^2} K_p}{h V_{p0}} & 1 & \frac{X_L}{h} k_p k_{pdc} & \frac{X_L}{h} k_p \\ \frac{-\sqrt{V_{p0}^2 V_0^2 - P_0^2 X_L^2} K_i}{h V_{p0}} & 0 & \frac{X_L}{h} k_i k_{pdc} & \frac{X_L}{h} k_i \\ \frac{I_{cd0} X_L}{h C V_{dc0}} \left(I_{q0} + \frac{X_L}{X_{ss}} I_{d0} \right) & 0 & \frac{-k_{dcp} V_{p0}}{C V_{dc0}} & \frac{-V_{p0}}{C V_{dc0}} \\ 0 & 0 & k_{dci} & 0 \end{bmatrix}$$

$$\boldsymbol{B_D} = \begin{bmatrix} \frac{-\sin\theta_{p0} K_p}{h} & \frac{\cos\theta_{p0} K_p}{h} \\ \frac{-\sin\theta_{p0} K_i}{h} & \frac{\cos\theta_{p0} K_i}{h} \\ \frac{-I_{cd0}}{C V_{dc0}} \cos\theta_{p0} & \frac{-I_{cd0}}{C V_{dc0}} \sin\theta_{p0} \\ 0 & 0 \end{bmatrix}$$

$$\boldsymbol{C_D} = \begin{bmatrix} -I_{y0} + \frac{\sqrt{V_{p0}^2 V_0^2 - P_0^2 X_L^2}}{h X_{ss}} \cos\theta_{p0} & 0 & \frac{k_{dcp}\cos\theta_{p0}}{h} & \frac{\cos\theta_{p0}}{h} \\ I_{x0} + \frac{\sqrt{V_{p0}^2 V_0^2 - P_0^2 X_L^2}}{h X_{ss}} \sin\theta_{p0} & 0 & \frac{k_{dcp}\sin\theta_{p0}}{h} & \frac{\sin\theta_{p0}}{h} \end{bmatrix}$$

$$\boldsymbol{D_D} = -\frac{1}{h X_{ss}} \begin{bmatrix} -\cos\theta_{p0}\sin\theta_{p0} & \cos^2\theta_{p0} \\ -\sin^2\theta_{p0} & \cos\theta_{p0}\sin\theta_{p0} \end{bmatrix} \tag{21}$$

where $h = 1 + \frac{X_L}{X_{ss}}$.

Denote $\lambda_{pll} = \xi_{pll} \pm j\omega_{pll}$ and $\lambda_{dc} = \xi_{dc} \pm j\omega_{dc}$ as the SSO modes of the DFIG subsystem dominated by both the PLL and DC voltage control. $\lambda_{pll} = \xi_{pll} \pm j\omega_{pll}$ and $\lambda_{dc} = \xi_{dc} \pm j\omega_{dc}$ are the two pairs of conjugate eigenvalues of $\boldsymbol{A_D}$ in (21). It can have

$$\begin{aligned}
\lambda_{pll} &= \xi_{pll} + j\omega_{pll} + \xi_{pll} - j\omega_{pll}\\
&\quad + \xi_{dc} + j\omega_{dc} + \xi_{dc} - j\omega_{dc} = 2(\xi_{pll} + \xi_{dc})\\
&= Trace(\boldsymbol{A_D}) = -\frac{\sqrt{V_{p0}^2 V_0^2 - P_0^2 X_L^2}}{h V_{p0}} K_p - \frac{k_{dcp} V_{p0}}{C V_{dc0}}
\end{aligned} \tag{22}$$

where $Trace(\boldsymbol{A_D})$ denotes the trace of $\boldsymbol{A_D}$, i.e., the summation of diagonal elements of $\boldsymbol{A_D}$.

From (22),

$$\begin{aligned}
&\frac{\partial}{\partial X_L} Trace(\boldsymbol{A_D})\\
&= \frac{K_p}{V_{p0}} \left(\frac{X_L}{h\sqrt{V_{p0}^2 V_0^2 - P_0^2 X_L^2}} + \frac{\sqrt{V_{p0}^2 V_0^2 - P_0^2 X_L^2}}{h^2 X_{ss}} \right) > 0
\end{aligned}$$

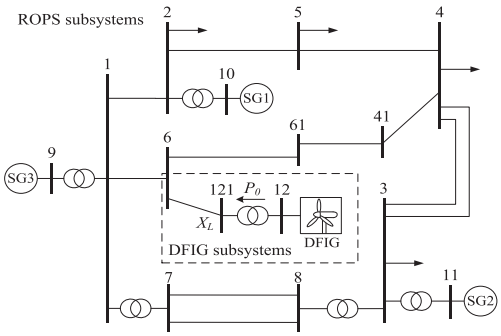

Fig. 4. Configuration of an example three-machine power system with the DFIG.

$$\frac{\partial}{\partial P_0} Trace(\boldsymbol{A_D}) = \frac{K_p}{V_{p0}} \cdot \frac{P_0}{h\sqrt{V_{p0}^2 V_0^2 - P_0^2 X_L^2}} > 0 \qquad (23)$$

From (23), it can be seen that when X_L or/and P_0 increase, $Trace(\boldsymbol{A_D})$ increases such that $\xi_{pll} + \xi_{dc}$ increases. Hence, when grid connection becomes weaker, damping of $\lambda_{pll} = \xi_{pll} \pm j\omega_{pll}$ or/and $\lambda_{dc} = \xi_{dc} \pm j\omega_{dc}$ decreases. The modal resonance may happen between the DFIG and the torsional dynamics of the SGs to lead to growing SSOs when their frequencies are approximately matched.

III. Study Cases

Fig. 4 shows the configuration of an example three-machine power system with a DFIG-based wind farm which is connected to grid via a transmission line represented by the lumped reactance X_L. The wind farm is comprised of 60 2 MW DFIGs. The wind farm is represented by an aggregated DFIG of 120MW. Details of the aggregated model of the wind farm are given in [21], [22]. In the following study cases, model and parameters of the DFIG given in [21] were adopted. Model and parameters of the SG recommended in [20] for the SSR study were used and adjusted according to the capacity of the SGs in the example power system. SG3 was a large grid and hence node 9 was an infinite busbar.

A. Study Cases About the SSO Mode Dominated by the PLL

In order to examine the instability mechanism associated with the PLL and DC voltage control, the commonly-used strategy is to change the PI gains of either the PLL or the DC voltage control [3]–[7]. For example, in [23], PI gains of the SRF PLL were varied from $K_p = 3, K_i = 0.14$ to $K_p = 60, K_i = 1400$ in order to examine the impact of the PLL on the system stability. Instability danger was identified when the PI gains were $K_p = 8, K_i = 25.6$. Hence, in the following study cases, the PI gains of the SRF PLL equipped by the DFIG in Fig. 3 were varied from $K_p = 3.4$ and $K_i = 15.5$ to $K_p = 4.5$ and $K_i = 42.5$. The SSO mode of DFIG subsystem dominated by the PLL, λ_{pll}, with the variation of PI gains of the SRF PLL was computed. Six study cases with different conditions of grid connection of the DFIG were: (1) Case 1: $X_L = 0.06$, $P_0 = 1.2$; (2) Case 2: $X_L = 0.17$, $P_0 = 1.2$; (3) Case 3: $X_L = 0.26$, $P_0 = 1.2$; (4) Case 4: $X_L = 0.26$, $P_0 = 0.75$; (5) Case 5: $X_L = 0.26$, $P_0 = 1.0$; (6) Case 6: $X_L = 0.26$, $P_0 = 1.2$.

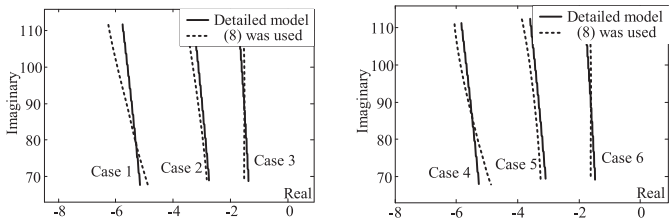

Fig. 5. Trajectories of SSO mode of DFIG subsystem dominated by the PLL when PI gains of PLL were varied.

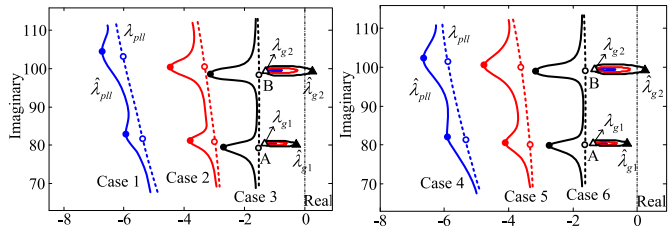

Fig. 6. Modal resonance affected by the condition of grid connection of DFIG when PI gains of PLL were varied.

In Fig. 5, dashed trajectories of λ_{pll} were computed by using the state matrix of simplified state-space model of DFIG subsystem derived in (12). Solid trajectories of λ_{pll} were calculated by using the detailed 18th-order state-space model of the DFIG with all the dynamics of the DFIG being included [21]. (Thus, the DFIG subsystem was of other oscillation modes in addition toλ_{pll}). Results in Fig. 5 firstly confirmed the correctness of model simplification made when the dominant SSO mode of the DFIG was associated with the PLL in section IIA. Secondly, they confirmed the conclusion made from (12) that when X_L or/and P_0 increased such that condition of grid connection became weaker, the SSO mode dominated by the PLL moved towards the right on the complex plane.

Fig. 6 presents the results to examine how the modal resonance between the DFIG and the SGs was affected by the variation of conditions of grid connection of the DFIG. In Fig. 6, hollow triangles indicate the positions of λ_{g1} and λ_{g2}, which were the first torsional SSO mode of SG1 and SG2 in the example three-machine power system. They were the SSO modes of ROPS subsystem. Dashed curves are the trajectories of λ_{pll} with the variation of PI gains of the PLL. Solid curves are the trajectories of SSO modes of the entire example power system with the dynamics of DFIG being included, denoted as $\hat{\lambda}_{g1}$, $\hat{\lambda}_{g2}$ and $\hat{\lambda}_{pll}$ in respective to λ_{g1}, λ_{g2} and λ_{pll} respectively. From Fig. 6, it can be seen that when X_L or/and P_0 increased such that the grid connection became weaker, λ_{pll} moved towards the right and closer to the lightly-damped λ_{g1} and λ_{g2}.

In Fig. 6, filled triangles and circles are the positions of $\hat{\lambda}_{g1}$, $\hat{\lambda}_{g2}$ and $\hat{\lambda}_{pll}$ when modal resonance happened. It can be seen that when the grid connection of the DFIG became weaker, the modal resonance was stronger such that the closed-loop torsional SSO modes, $\hat{\lambda}_{g1}$ and $\hat{\lambda}_{g2}$, moved further towards the right on the complex plane. When modal resonance happened at point B in Fig. 6 under the condition of weakest grid connection, the DFIG induced growing SSOs.

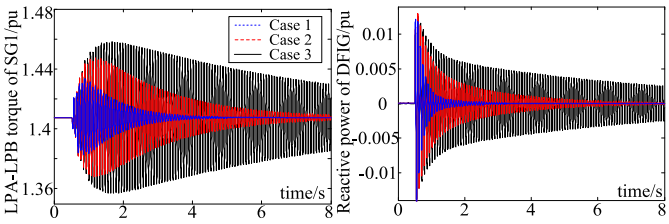

Fig. 7. Results of simulation when $K_p = 3.76$ and $K_i = 20.67$.

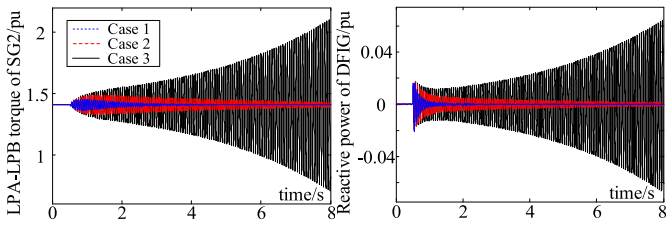

Fig. 8. Results of simulation when $K_p = 4.13$ and $K_i = 31.72$.

Results of simulation when $K_p = 3.76$ and $K_i = 20.67$ are presented in Fig. 7. Results of simulation when $K_p = 4.13$ and $K_i = 31.72$ are presented in Fig. 8. The simulation was conducted when the voltage at the terminal of DFIG dropped by 10% at 0.5 second of simulation and recovered in 0.01 second. Comprehensive high-order (the 18th-order) model of the DFIG was used in the simulation [21], which included the torsional dynamics of wind turbine, transient of stator and rotor windings of the DFIG, dynamics of the rotor side converter and grid side converter as well as the associated converter control systems, the transient of output filter. The For comparison, results of simulation in case 1 and case 2 are also given in Fig. 7 and Fig. 8. Simulation presented in Fig. 7 and Fig. 8 was conducted with full 18th-order model of DFIG being used. From Fig. 7 and 8, it can be observed that more damping degradation of torsional SSO modes of the SGs occurred when the grid connection of the DFIG was weaker. Particularly, growing SSOs were induced in case 3 (weakest grid connection) in the example power system when $K_p = 4.13$ and $K_i = 31.72$ (Fig. 8).

B. Study Cases About SSO Mode Dominated by the DC Voltage Control

In [23], danger of oscillation instability was detected when the PI gains of the DC voltage control were $K_{dcp} = 8$ and $K_{dci} = 400$. In the following study cases, PI gains of the DC voltage control of the DFIG were varied from $K_{dcp} = 40$ and $K_{dci} = 130$ to $K_{dcp} = 63$ and $K_{dci} = 368$. The proportional gain was bigger than the setting given in [23] and hence damping of the SSO mode associated with the DC voltage control was better than that in [23]. The SSO mode of DFIG subsystem dominated by the DC voltage control, λ_{dc}, with the variation of PI gains of DC voltage control was computed. Following six study cases with different conditions of grid connection of the DFIG were examined: (1) Case 7: $X_L = 0.08$, $P_0 = 1.2$; (2) Case 8: $X_L = 0.17$, $P_0 = 1.2$; (3) Case 9: $X_L = 0.22$, $P_0 = 1.2$; (4) Case 10: $X_L = 0.22$, $P_0 = 0.9$; (5) Case 11: $X_L = 0.22$, $P_0 = 1.1$; (6) Case 12: $X_L = 0.22$, $P_0 = 1.2$.

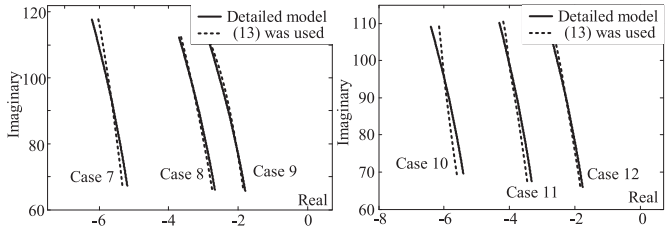

Fig. 9. Trajectories of SSO mode of the DFIG subsystem dominated by the DC voltage control when PI gains of DC voltage control were varied.

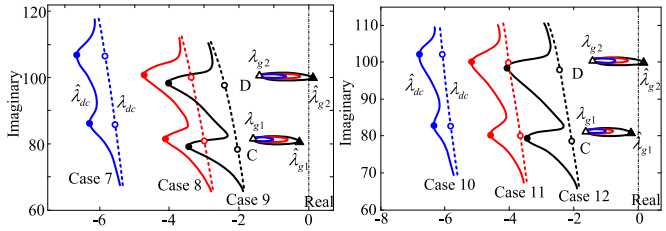

Fig. 10. Modal resonance affected by the condition of grid connection of DFIG when PI gains of DC voltage control of DFIG were varied.

In Fig. 9, dashed trajectories of λ_{dc} were computed by using the simplified state-space model of DFIG subsystem derived in (17). Solid trajectories of λ_{dc} were calculated using the detailed 18th-order state-space model of the DFIG with all dynamics of the DFIG being included (Thus, the DFIG subsystem was of other oscillation modes in addition to λ_{dc}) [21]. Results in Fig. 9 firstly confirmed the correctness of model simplification made when the dominant SSO mode of the DFIG was associated with the DC voltage control in section IIB. Secondly, they confirmed the conclusion made from (17) that when X_L or/and P_0 increased such that the grid connection became weaker, the SSO mode of DFIG subsystem dominated by the DC voltage control of the DFIG moved towards the right on the complex plane.

In Fig. 10, hollow triangles are the positions of λ_{g1} and λ_{g2}, the first torsional SSO mode of SG1 and SG2 in the example three-machine power system respectively. They were the SSO mode of ROPS subsystem. Dashed curves are the trajectories of λ_{dc} with the variation of PI gains of the DC voltage control of the DFIG. λ_{dc} was the SSO mode of DFIG subsystem. Solid curves are the trajectories of SSO modes of the entire example power system with dynamics of DFIG being included, denoted as $\hat{\lambda}_{g1}$, $\hat{\lambda}_{g2}$ and $\hat{\lambda}_{dc}$. It can be seen that when X_L or/and P_0 increased such that the grid connection became weaker, λ_{dc} moved towards the right and closer to the lightly-damped λ_{g1} and λ_{g2}. Consequently, modal resonance happened when the frequency of λ_{dc} approximately matched the frequencies of λ_{g1} and λ_{g2}. In addition, modal resonance became stronger under the conditions of weaker grid connection such that $\hat{\lambda}_{g1}$ and $\hat{\lambda}_{g2}$ moved further towards the right on the complex plane. When modal resonance happened at point D in Fig. 10, the DFIG induced growing SSOs under the condition of weakest grid connection.

In Fig. 10, when $K_{dcp} = 36.08$ and $K_{dci} = 198.54$, λ_{dc} was at point C in case 9 where $\lambda_{dc} = -2.04 + j78.4$. When

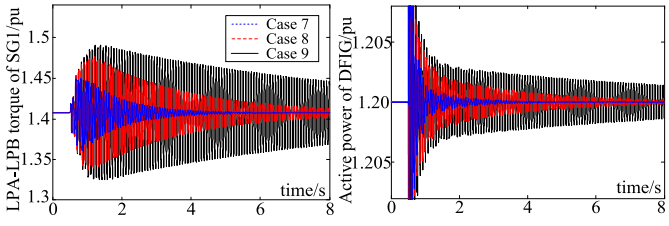

Fig. 11. Results of simulation when $K_{dcp} = 36.08$ and $K_{dci} = 198.54$.

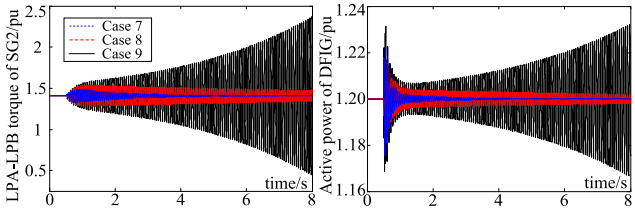

Fig. 12. Results of simulation when $K_{dcp} = 54.25$ and $K_{dci} = 284.49$.

$K_{dcp} = 54.25$ and $K_{dci} = 284.49$, λ_{dc} was at point D in case 9. where $\lambda_{dc} = -2.41 + j97.6$. Results of simulation when $K_{dcp} = 36.08$ and $K_{dci} = 198.54$ are presented in Fig. 11. Results of simulation when $K_{dcp} = 54.25$ and $K_{dci} = 284.49$ are presented in Fig. 12. The simulation was conducted when the mechanical torque input to DFIG increased by 10% at 0.5 second of simulation and recovered in 0.01 second. High-order model of the DFIG [21] was used for the simulation. For comparison, results of simulation in case 7 and case 8 are also given in Fig. 11 and Fig. 12. Simulation was conducted with full 18th-order model of DFIG being used. Hence, the simulation confirmed that the dynamics of the DFIG with full detailed model being used was dominated by the SSO mode associated with the DC voltage control, λ_{dc}.

From Fig. 11 and 12, it can be observed that more damping degradation of torsional SSO modes of the SGs occurred when the grid connection of the DFIG was weaker. Particularly, growing SSOs were induced by the DFIG in case 9 in the example power system when the condition of grid connection was the weakest and modal resonance was the strongest.

IV. Conclusion

This paper has carried out the analytical examination on the role played by the condition of weak grid connection for a grid-connected DFIG to "excite" the torsional dynamics of the SGs. The examination explains why the DFIG is more likely to induce torsional SSOs under the condition of weak grid connection. Novel contributions made by the paper are summarized as follows.

1) Theoretical analysis is presented to prove that the weak grid connection amplifies the impact of modal resonance between the DFIG and torsional dynamics of the SGs. Consequently, under the condition of weak grid connection, the DFIG may more likely cause growing torsional SSOs when the modal resonance happens. Hence, the analysis in the paper provides an explanation about the SSO incidents in Harmi power system, China, from the perspective of amplifying effect of weak grid connection of DFIG.
2) In order to conduct theoretical examination, analysis in the paper has focused on the SSO mode of DFIG dominated by the PLL and DC voltage control of DFIG. Analytical conclusions obtained are evaluated by using an example power system when detailed model of DFIG was used. Hence, in the evaluation, dynamics of both the PLL and DC voltage control were included, in addition to all the other dynamics of DFIG. Results of evaluation have confirmed the correctness of theoretical analysis.

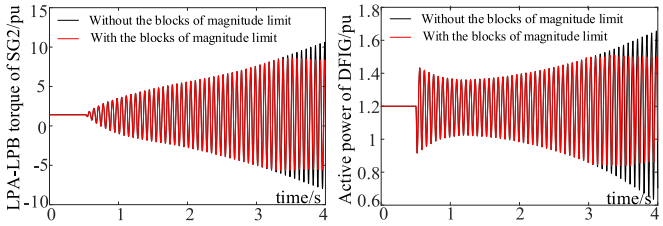

Fig. 13. Results of simulation with and without magnitude limit blocks.

Theoretical analysis in the paper contributes to the revelation of mechanism about why under the condition of weak grid connection, the grid-connected DFIG may intend to introduce the risk of torsional SSOs. Thus, a deeper insight and better understanding about the impact of condition of weak grid connection are provided. Study in the paper focuses on the dynamics of PLL and the DC voltage control, as it has been found in the literature that the PLL and DC voltage control may more possibly be responsible for the DFIG to induce the torsional SSOs under the condition of weak grid connection. Hence, the analytical conclusions obtained in the paper are limited to the impact of the PLL and DC voltage control.

In the literature, the SSOs have been investigated by using the linearized model of a power system. Hence, the investigation carried out so far has been about the small-signal stability of the power system with the nonlinear components in the power system being neglected. However, when growing SSOs occur, i.e., the power system is unstable, some of non-linear components may function to affect the SSOs. The function cannot be properly reflected by using the linearized model of the power system. This is the limitation of small-signal stability analysis, though the analysis has been widely practiced and accepted in the study of power system SSOs.

To demonstrate the effect of non-linear components, the blocks of magnitude limit on the current control loops of the converter of the DFIG in the example power system of Fig. 4 were added in the high-order model of the DFIG. Simulation was conducted when the mechanical torque input to DFIG increased by 30% at 0.5 second of simulation and recovered in 0.01 second. Results of simulation are presented in Fig. 13. For comparison, results of simulation without the blocks of magnitude limit are also presented in Fig. 13. It can be seen that the SSOs were constrained by the magnitude limit such that the sustained SSOs instead of growing SSOs were observed when the blocks of magnitude limit functioned.

APPENDIX A

Linearized relations between the stator and rotor current are [24]

$$\Delta I_{sd} = \frac{X_m}{X_{ss}}\Delta I_{rd} - \frac{1}{X_{ss}}\Delta V_{pq}, \Delta I_{sq} = \frac{X_m}{X_{ss}}\Delta I_{rq} + \frac{1}{X_{ss}}\Delta V_{pd} \tag{A1}$$

where $I_{sd} + jI_{sq}$ and $I_{rd} + jI_{rq}$ respectively are the stator and rotor current expressed in the $d-q$ of the DFIG; X_{ss} is the self-inductance of stator windings; X_m is the magnetizing inductance.

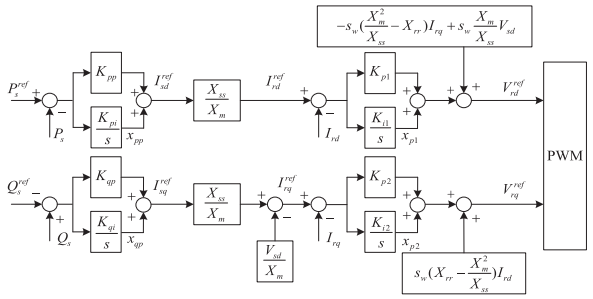

Fig. A1. Control system of RSC.

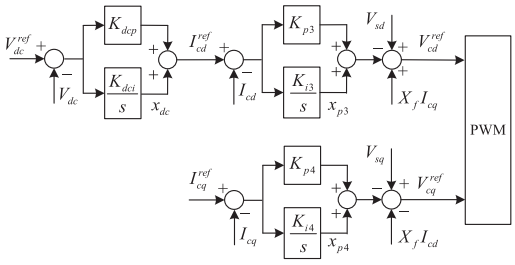

Fig. A2. Control system of GSC.

Configurations of control systems of the RSC and GSC of the DFIG are shown by Fig. A1 and A2 respectively. Ignoring the transient of control system of the RSC, from Fig. A1,

$$\Delta I_{rd} \approx 0, \Delta I_{rq} \approx -\frac{1}{X_m}\Delta V_{pd} \tag{A2}$$

Ignoring the dynamics of rotor motion of the DFIG [25], linearized equation of active power output from the DFIG is

$$\Delta P = I_{d0}\Delta V_{pd} + V_{p0}\Delta I_d + I_{q0}\Delta V_{pq} \approx \omega_{r0}\Delta P_s \tag{A3}$$

where ω_r is the rotor speed of the DFIG. From (A3),

$$I_{d0}\Delta V_{pd} + V_{p0}\Delta I_d + I_{q0}\Delta V_{pq} = \omega_{r0}(I_{sd0}\Delta V_{pd} + V_{p0}\Delta I_{sd} + I_{sq0}\Delta V_{pq}) \tag{A4}$$

Substituting (A2) in (A1), it can have $\Delta I_{sq} \approx 0$, $\Delta I_{sd} = -\frac{1}{X_{ss}}\Delta V_{pq}$, and $I_{d0} \approx \omega_{r0} I_{sd0}$. From (A4),

$$V_{p0}\Delta I_d + I_{q0}\Delta V_{pq} = \omega_{r0}\left(I_{sq0} - \frac{V_{p0}}{X_{ss}}\right)\Delta V_{pq} \tag{A5}$$

Thus, from (A5),

$$\Delta I_d = \left(\frac{\omega_{r0} I_{sq0} - I_{q0}}{V_{pd0}} - \frac{\omega_{r0}}{X_{ss}}\right)\Delta V_{pq} = \kappa \Delta V_{pq}, \Delta I_q = 0 \tag{A6}$$

Linearized transformation equations between the $d-q$ and $x-y$ coordinate are

$$\begin{cases} \begin{bmatrix}\Delta I_x \\ \Delta I_y\end{bmatrix} = \begin{bmatrix}\cos\theta_{p0} & -\sin\theta_{p0} \\ \sin\theta_{p0} & \cos\theta_{p0}\end{bmatrix}\begin{bmatrix}\Delta I_d \\ \Delta I_q\end{bmatrix} + \begin{bmatrix}-I_{y0} \\ I_{x0}\end{bmatrix}\Delta\theta_{pll} \\ \begin{bmatrix}\Delta V_{pd} \\ \Delta V_{pq}\end{bmatrix} = \begin{bmatrix}\cos\theta_{p0} & \sin\theta_{p0} \\ -\sin\theta_{p0} & \cos\theta_{p0}\end{bmatrix}\begin{bmatrix}\Delta V_{px} \\ \Delta V_{py}\end{bmatrix} + \begin{bmatrix}V_{q0} \\ -V_{d0}\end{bmatrix}\Delta\theta_{pll} \end{cases} \tag{A7}$$

From (A6) and (A7),

$$\begin{cases} \begin{bmatrix}\Delta I_x \\ \Delta I_y\end{bmatrix} = \begin{bmatrix}\kappa\cos\theta_{p0} \\ \kappa\sin\theta_{p0}\end{bmatrix}\Delta V_{pq} + \begin{bmatrix}-I_{y0} \\ I_{x0}\end{bmatrix}\Delta\theta_{pll} \\ \Delta V_{pq} = \begin{bmatrix}-\sin\theta_{p0} & \cos\theta_{p0}\end{bmatrix}\begin{bmatrix}\Delta V_{px} \\ \Delta V_{py}\end{bmatrix} - V_{p0}\Delta\theta_{pll} \end{cases} \tag{A8}$$

From (A8),

$$\begin{bmatrix}\Delta I_x \\ \Delta I_y\end{bmatrix} = \begin{bmatrix}-\kappa V_{p0}\cos\theta_{p0} - I_{y0} \\ -\kappa V_{p0}\sin\theta_{p0} + I_{x0}\end{bmatrix}\Delta\theta_{pll} + \begin{bmatrix}-\kappa\cos\theta_{p0}\sin\theta_{p0} & \kappa\cos^2\theta_{p0} \\ -\kappa\sin^2\theta_{p0} & \kappa\cos\theta_{p0}\sin\theta_{p0}\end{bmatrix}\begin{bmatrix}\Delta V_{px} \\ \Delta V_{py}\end{bmatrix} \tag{A9}$$

From (11) and (A9), it can have

$$\begin{bmatrix}1-\kappa X_L\sin^2\theta_{p0} & \kappa X_L\cos\theta_{p0}\sin\theta_{p0} \\ \kappa X_L\cos\theta_{p0}\sin\theta_{p0} & 1-\kappa X_L\cos^2\theta_{p0}\end{bmatrix}\begin{bmatrix}\Delta V_{px} \\ \Delta V_{py}\end{bmatrix} = \begin{bmatrix}\Delta V_x \\ \Delta V_y\end{bmatrix} + \begin{bmatrix}(\kappa V_{p0}\sin\theta_{p0} + I_{x0})X_L \\ -(\kappa V_{p0}\cos\theta_{p0} + I_{y0})X_L\end{bmatrix}\Delta\theta_{pll} \tag{A10}$$

where,

$$\begin{bmatrix}1-\kappa X_L\sin^2\theta_{p0} & \kappa X_L\cos\theta_{p0}\sin\theta_{p0} \\ \kappa X_L\cos\theta_{p0}\sin\theta_{p0} & 1-\kappa X_L\cos^2\theta_{p0}\end{bmatrix}^{-1} = \frac{1}{m}\begin{bmatrix}1-\kappa X_L\cos^2\theta_{p0} & -\kappa X_L\cos\theta_{p0}\sin\theta_{p0} \\ -\kappa X_L\cos\theta_{p0}\sin\theta_{p0} & 1-\kappa X_L\sin^2\theta_{p0}\end{bmatrix}$$

$$m = 1-\kappa X_L = \frac{X_{ss}+\omega_{r0}X_L}{X_{ss}} + \frac{1-\omega_{r0}}{V_{p0}}I_{sq0}X_L \tag{A11}$$

Substituting $I_{sq0}X_L = -\frac{Q_0 X_L}{V_{p0}} = -\frac{V_{p0}^2 - \sqrt{V_{p0}^2V_0^2 - P_0^2X_L^2}}{V_{p0}}$ in (A11)

$$m = \frac{1}{V_{p0}^2}\left[\frac{X_{ss}+X_L}{X_{ss}}\omega_{r0}V_{p0}^2 + (1-\omega_{r0})\sqrt{V_{p0}^2V_0^2 - P_0^2X_L^2}\right] = \frac{1}{V_{p0}^2}\alpha \tag{A12}$$

From (A10),

$$\begin{bmatrix}\Delta V_{px} \\ \Delta V_{py}\end{bmatrix} = \frac{X_L}{m}\begin{bmatrix}\kappa V_{p0}\sin\theta_{p0} - I_{x0} + \kappa I_{d0}X_L\cos\theta_{p0} \\ -\kappa V_{p0}\cos\theta_{p0} - I_{y0} + \kappa I_{d0}X_L\sin\theta_{p0}\end{bmatrix}\Delta\theta_{pll}$$

$$+\frac{1}{m}\begin{bmatrix} 1-\kappa X_L\cos^2\theta_{p0} & -\kappa X_L\cos\theta_{p0}\sin\theta_{p0} \\ -\kappa X_L\cos\theta_{p0}\sin\theta_{p0} & 1-\kappa X_L\sin^2\theta_{p0}\end{bmatrix}\begin{bmatrix}\Delta V_x\\ \Delta V_y\end{bmatrix} \tag{A13}$$

Substituting (A13) in the second equation of (A8),

$$\Delta V_{pq} = -\frac{V_{p0}\sqrt{V_{p0}^2V_0^2-P_0^2X_L^2}}{\alpha}\Delta\theta_{pll} + \frac{1}{m}\begin{bmatrix}-\sin\theta_{p0} & \cos\theta_{p0}\end{bmatrix}\begin{bmatrix}\Delta V_x\\ \Delta V_y\end{bmatrix} \tag{A14}$$

Substituting (A14) in the first equation of (A8),

$$\begin{bmatrix}\Delta I_x\\ \Delta I_y\end{bmatrix} = -\frac{V_{p0}+I_{q0}X_L}{m}\begin{bmatrix}\kappa\cos\theta_{p0}\\ \kappa\sin\theta_{p0}\end{bmatrix}\Delta\theta_{pll} + \begin{bmatrix}-I_{y0}\\ I_{x0}\end{bmatrix}\Delta\theta_{pll} + \frac{1}{m}\begin{bmatrix}-\kappa\cos\theta_{p0}\sin\theta_{p0} & \kappa\cos^2\theta_{p0}\\ -\kappa\sin^2\theta_{p0} & \kappa\cos\theta_{p0}\sin\theta_{p0}\end{bmatrix}\begin{bmatrix}\Delta V_x\\ \Delta V_y\end{bmatrix} \tag{A15}$$

Substituting (A14) in (10), $\boldsymbol{A}_D$ and $\boldsymbol{B}_D$ in (12) are obtained. From (A15), $\boldsymbol{C}_D$ and $\boldsymbol{D}_D$ in (12) are obtained.

APPENDIX B

From Fig. A2,

$$\Delta I_{cd} = K_{dcp}\Delta V_{dc} + \Delta x_{dc}, \Delta I_{cq} \approx 0 \tag{B1}$$

The linearized equation of active power injected into the GSC from the DC side (see Fig. 1) is

$$\Delta P_c = V_{pd0}\Delta I_{cd} + I_{cd0}\Delta V_{pd} \tag{B2}$$

As only the dynamics of DC voltage are considered, it can have that $\Delta I_{cd} \approx \Delta I_d$, $\Delta I_{cq} \approx \Delta I_q$.

Linearized equation of phase of the terminal voltage of the DFIG is

$$\Delta\theta_p = \begin{bmatrix}-\frac{V_{py0}}{V_{p0}^2} & \frac{V_{px0}}{V_{p0}^2}\end{bmatrix}\begin{bmatrix}\Delta V_{px}\\ \Delta V_{py}\end{bmatrix} \tag{B3}$$

For an ideal PLL, $\Delta\theta_{pll} \approx \Delta\theta_p$. Thus, from (A7) and (B3),

$$\begin{bmatrix}\Delta I_x\\ \Delta I_y\end{bmatrix} = \begin{bmatrix}\cos\theta_{p0} & -\sin\theta_{p0}\\ \sin\theta_{p0} & \cos\theta_{p0}\end{bmatrix}\begin{bmatrix}\Delta I_d\\ \Delta I_q\end{bmatrix} + \begin{bmatrix}\frac{V_{py0}I_{y0}}{V_{p0}^2} & -\frac{V_{px0}I_{y0}}{V_{py0}^2}\\ -\frac{V_{py0}I_{x0}}{V_{py0}^2} & \frac{V_{px0}I_{x0}}{V_{py0}^2}\end{bmatrix}\begin{bmatrix}\Delta V_{px}\\ \Delta V_{py}\end{bmatrix} \tag{B4}$$

From (11), (B1) and (B4),

$$\begin{bmatrix}\Delta I_x\\ \Delta I_y\end{bmatrix} = \beta\begin{bmatrix}K_{dcp}\left(\cos\theta_{p0}-\frac{V_{py0}I_{d0}}{V_{p0}^2}X_L\right) & \cos\theta_{p0}-\frac{V_{py0}I_{d0}}{V_{p0}^2}X_L\\ K_{dcp}\left(\sin\theta_{p0}+\frac{V_{px0}I_{d0}}{V_{p0}^2}X_L\right) & \sin\theta_{p0}+\frac{V_{px0}I_{d0}}{V_{p0}^2}X_L\end{bmatrix}\begin{bmatrix}\Delta V_{dc}\\ \Delta x_{dc}\end{bmatrix} + \begin{bmatrix}\frac{V_{py0}I_{y0}}{V_{p0}^2} & -\frac{V_{px0}I_{y0}}{V_{p0}^2}\\ -\frac{V_{py0}I_{x0}}{V_{p0}^2} & \frac{V_{px0}I_{x0}}{V_{p0}^2}\end{bmatrix}\begin{bmatrix}\Delta V_x\\ \Delta V_y\end{bmatrix} \tag{B5}$$

where, $\beta = \frac{V_{p0}^2}{V_{p0}^2-Q_0X_L} = \frac{V_{p0}^2}{\sqrt{V_{p0}^2V_0^2-P_0^2X_L^2}} = \frac{V_{p0}^2}{c}$;

$$\cos\theta_{p0} - \frac{V_{py0}I_{d0}}{V_{p0}^2}X_L = \frac{V_{p0}^2V_{px0}+V_{py0}^2V_{x0}+V_{px0}V_{py0}V_{y0}}{V_{p0}^3}$$

$$\sin\theta_{p0} + \frac{V_{px0}I_{d0}}{V_{p0}^2}X_L = \frac{V_{p0}^2V_{py0}-V_{px}^2V_{y0}+V_{px0}V_{py0}V_{x0}}{V_{p0}^3}.$$

From (11) and the second equation of (A7),

$$\Delta V_{pd} = \begin{bmatrix}\cos\theta_{p0} & \sin\theta_{p0}\end{bmatrix}\begin{bmatrix}\Delta V_{px}\\ \Delta V_{py}\end{bmatrix} = \begin{bmatrix}\frac{V_{py0}}{V_{p0}}X_L & -\frac{V_{px0}}{V_{p0}}X_L\end{bmatrix}\begin{bmatrix}\Delta I_x\\ \Delta I_y\end{bmatrix} + \begin{bmatrix}\frac{V_{px0}}{V_{p0}} & \frac{V_{py0}}{V_{p0}}\end{bmatrix}\begin{bmatrix}\Delta V_x\\ \Delta V_y\end{bmatrix} \tag{B6}$$

Substituting (B5) in (B6),

$$\Delta V_{pd} = \begin{bmatrix}\cos\theta_{p0} & \sin\theta_{p0}\end{bmatrix}\begin{bmatrix}\Delta V_{px}\\ \Delta V_{py}\end{bmatrix} = \beta\begin{bmatrix}-\frac{I_{d0}X_L^2}{V_{p0}}K_{pdc} & -\frac{I_{d0}X_L^2}{V_{p0}}\end{bmatrix}\begin{bmatrix}\Delta V_{dc}\\ \Delta x_{dc}\end{bmatrix} + \begin{bmatrix}\frac{V_{p0}V_{x0}}{V_{p0}^2-Q_0X_L} & \frac{V_{p0}V_{y0}}{V_{p0}^2-Q_0X_L}\end{bmatrix}\begin{bmatrix}\Delta V_x\\ \Delta V_y\end{bmatrix} \tag{B7}$$

Substituting (B7) in (16), $\boldsymbol{A}_D$ and $\boldsymbol{B}_D$ in (17) are obtained. From (B5), $\boldsymbol{C}_D$ and $\boldsymbol{D}_D$ in (17) are obtained.

APPENDIX C

Combining (A1), (A2) and (B1),

$$\Delta I_d = \Delta I_{sd} + \Delta I_{cd} = -\frac{1}{X_{ss}}\Delta V_{pq} + K_{dcp}\Delta V_{dc} + \Delta x_{dc}$$

$$\Delta I_q = \Delta I_{sq} + \Delta I_{cq} = 0 \tag{C1}$$

From (A7) and (C1),

$$\begin{bmatrix}\Delta I_x\\ \Delta I_y\end{bmatrix} = \begin{bmatrix}k_{dcp}\cos\theta_{p0} & \cos\theta_{p0}\\ k_{dcp}\sin\theta_{p0} & \sin\theta_{p0}\end{bmatrix}\begin{bmatrix}\Delta V_{dc}\\ \Delta x_{dc}\end{bmatrix} + \begin{bmatrix}-I_{y0}+\frac{V_{p0}\cos\theta_{p0}}{X_{ss}}\\ I_{x0}+\frac{V_{p0}\sin\theta_{p0}}{X_{ss}}\end{bmatrix}\Delta\theta_{pll} - \begin{bmatrix}-\frac{1}{X_{ss}}\cos\theta_{p0}\sin\theta_{p0} & \frac{1}{X_{ss}}\cos^2\theta_{p0}\\ -\frac{1}{X_{ss}}\sin^2\theta_{p0} & \frac{1}{X_{ss}}\cos\theta_{p0}\sin\theta_{p0}\end{bmatrix}\begin{bmatrix}\Delta V_{px}\\ \Delta V_{py}\end{bmatrix} \tag{C2}$$

From (11) and (C2), it can have

$$\begin{bmatrix}\Delta V_{px}\\ \Delta V_{py}\end{bmatrix} = \frac{X_L}{h}\begin{bmatrix}\dfrac{-V_{p0}\sin\theta_{p0}}{X_{ss}} - I_{x0} - \dfrac{I_{d0}X_L\cos\theta_{p0}}{X_{ss}}\\ \dfrac{V_{p0}\sin\theta_{p0}}{X_{ss}} - I_{y0} - \dfrac{I_{d0}X_L\sin\theta_{p0}}{X_{ss}}\end{bmatrix}\Delta\theta_{pll} + \frac{X_L}{h}\begin{bmatrix}-k_p\sin\theta_{p0} & -\sin\theta_{p0}\\ k_p\cos\theta_{p0} & \cos\theta_{p0}\end{bmatrix}\begin{bmatrix}\Delta V_{dc}\\ \Delta x_{dc}\end{bmatrix} + \frac{1}{h}\begin{bmatrix}1+\dfrac{X_L\cos^2\theta_{p0}}{X_{ss}} & \dfrac{X_L\cos\theta_{p0}\sin\theta_{p0}}{X_{ss}}\\ \dfrac{X_L\cos\theta_{p0}\sin\theta_{p0}}{X_{ss}} & 1+\dfrac{X_L\sin^2\theta_{p0}}{X_{ss}}\end{bmatrix} \times \begin{bmatrix}\Delta V_x\\ \Delta V_y\end{bmatrix} \tag{C3}$$

where $h = 1 + \frac{X_L}{X_{ss}}$.

Substituting (C3) in (C2), $\boldsymbol{C}_D$ and $\boldsymbol{D}_D$ in (21) are obtained

$$\begin{bmatrix}\Delta I_x\\ \Delta I_y\end{bmatrix} = \frac{1}{h}\begin{bmatrix}k_{dcp}\cos\theta_{p0} & \cos\theta_{p0}\\ k_{dcp}\sin\theta_{p0} & \sin\theta_{p0}\end{bmatrix}\begin{bmatrix}\Delta V_{dc}\\ \Delta x_{dc}\end{bmatrix} + \begin{bmatrix}-I_{y0} + \dfrac{V_{p0}+I_{q0}X_L}{hX_{ss}}\cos\theta_{p0}\\ I_{x0} + \dfrac{V_{p0}+I_{q0}X_L}{hX_{ss}}\sin\theta_{p0}\end{bmatrix}\Delta\theta_{pll} - \frac{1}{hX_{ss}}\begin{bmatrix}-\cos\theta_{p0}\sin\theta_{p0} & \cos^2\theta_{p0}\\ -\sin^2\theta_{p0} & \cos\theta_{p0}\sin\theta_{p0}\end{bmatrix}\begin{bmatrix}\Delta V_{px}\\ \Delta V_{py}\end{bmatrix} \tag{C4}$$

From (10), (A7) and (C3), the 1st and 2nd row elements of matrices $\boldsymbol{A}_D$ and $\boldsymbol{B}_D$ in (21) are obtained. From (17), (B2) and (C3), the 3th and 4th row elements of matrices $\boldsymbol{A}_D$ and $\boldsymbol{B}_D$ in (21) are obtained.

REFERENCES

[1] N. P. W. Strachan and D. Jovcic, "Stability of a variable-speed permanent magnet wind generator with weak AC grids," *IEEE Trans. Power Del.*, vol. 25, no. 4, pp. 2779–2788, Oct. 2010.

[2] Y. Huang, X. Yuan, J. Hu, and P. Zhou, "Modeling of VSC connected to weak grid for stability analysis of DC-link voltage control," in *IEEE J. Emerg. Sel. Topics Power Electron.*, vol. 3, no. 4, pp. 1193–1204, Dec. 2015.

[3] J. Liu *et al.*, "Impact of power grid strength and PLL parameters on stability of grid-connected DFIG wind farm," *IEEE Trans. Sustain. Energy*, to be published, doi 10.1109/TSTE.2019.2897596.

[4] X. Xi, H. Geng, and G. Yang, "Modelling of the DFIG based wind farms for small signal stability analysis of weak power grids," in *Proc. 2nd IET Renewable Power Gener. Conf.*, Beijing, 2013, pp. 1–4.

[5] J. Hu, Y. Huang, D. Wang, H. Yuan, and X. Yuan, "Modeling of grid-connected DFIG-based wind turbines for DC-link voltage stability analysis," *IEEE Trans. Sustain. Energy*, vol. 6, no. 4, pp. 1325–1336, Oct. 2015.

[6] M. Wan and J. Hu, "Modal analysis of a grid-connected DFIG-based WT considering multi-timescale control interactions," in *J. Eng.*, vol. 2017, no. 13, pp. 1118–1123, 2017.

[7] D. Wang, Yunhe Hou, and J. Hu, "Stability of DC-link voltage control for paralleled DFIG-based wind turbines connected to weak AC grids," in *Proc. IEEE Power Energy Soc. Gen. Meeting*, Boston, MA, 2016, pp. 1–5.

[8] D. Wang, L. Liang, L. Shi, J. Hu, and Y. Hou, "Analysis of modal resonance between PLL and DC-link voltage control in weak-grid tied VSCs," *IEEE Trans. Power Syst.*, vol. 34, no. 2, pp. 1127–1138, Mar. 2019.

[9] L. Fan, "Modeling type-4 wind in weak grids," *IEEE Trans. Sustain. Energy*, vol. 10, no. 2, pp. 853–864, Apr. 2019.

[10] L. Fan and Z. Miao, "An explanation of oscillations due to wind power plants weak grid interconnection," *IEEE Trans. Sustain. Energy*, vol. 9, no. 1, pp. 488–490, Jan. 2018.

[11] H. Liu *et al.*, "Subsynchronous interaction between direct-drive PMSG based wind farms and weak AC networks," *IEEE Trans. Power Syst.*, vol. 32, no. 6, pp. 4708–4720, Nov. 2017.

[12] W. Du, C. Chen, and H. Wang, "Sub-synchronous interactions induced by DFIGs in power systems without series compensated lines," *IEEE Trans. Sustain. Energy*, vol. 9, no. 3, pp. 1275–1284, 2018.

[13] W. Du, X. Chen, and H. Wang, "A method of open-loop modal analysis to examine the SSOs in a multi-machine power system with multiple variable-speed wind generators," *IEEE Trans. Power Syst.*, vol. 33, no. 4, pp. 4297–4307, Jul. 2018.

[14] F. Golnaraghi and B. C. Kuo, *Automatic Control Systems*, 9th ed. Hoboken, NJ, USA: Wiley, 2010.

[15] *IEEE Guide for Planning DC Links Terminating at AC Locations Having Low Short-Circuit Capacities*, IEEE Std 1204-1997, 21 Jan. 1997.

[16] W. Du, B. Ren, H. Wang, and Y. Wang, "Comparison of methods to examine sub-synchronous oscillations caused by grid-connected wind turbine generators," *IEEE Trans. Power Syst.*, vol. 34, no. 6, pp. 4931–4943, Nov. 2019.

[17] S. Golestan, J. M. Guerrero, A. Vidal, A. G. Yepes, and J. Doval-Gandoy, "PLL with MAF-based prefiltering stage: Small-signal modeling and performance enhancement," *IEEE Trans. Power Electron.*, vol. 31, no. 6, pp. 4013–4019, Jun. 2016.

[18] Y. Han, M. Luo, X. Zhao, J. M. Guerrero, and L. Xu, "Comparative performance evaluation of orthogonal-signal-generators-based single- phase PLL algorithms—A survey," *IEEE Trans. Power Electron.*, vol. 31, no. 5, pp. 3932–3944, May 2016.

[19] S.-K. Chung, "A phase tracking system for three phase utility interface inverters," *IEEE Trans. Power Electron.*, vol. 15, no. 3, pp. 431–438, May 2000.

[20] IEEE Subsynchronous Resonance Task Force, "First benchmark model for computer simulation of subsynchronous resonance," *IEEE Trans. Power App. Syst.*, vol. 96, no. 5, pp. 1565–1572, Sep. 1977.

[21] L. Fan, R. Kavasseri, Z. L. Miao, and C. Zhu, "Modeling of DFIG-based wind farms for SSR analysis," *IEEE Trans. Power Del.*, vol. 25, no. 4, pp. 2073–2082, Oct. 2010.

[22] W. Du, W. Dong, H. Wang, and J. Cao, "Dynamic aggregation of same wind turbine generators in parallel connection for studying oscillation stability of a wind farm," *IEEE Trans. Power Syst.*, vol. 34, no. 6, pp. 4694–4705, Nov. 2019.

[23] W. He, X. Yuan, and J. Hu, "Inertia provision and estimation of PLL-based DFIG wind turbines," *IEEE Trans. Power Syst.*, vol. 32, no. 1, pp. 510–521, Jan. 2017.

[24] A. Feijóo, J. Cidrás, and C. Carrillo, "A third order model for the doubly-fed induction machine," *Electric Power Syst. Res.*, vol. 56, no. 2, p. 121, Nov. 2000.

[25] Q. Hu, J. Hu, H. Yuan, H. Tang, and Y. Li, "Synchronizing stability of DFIG-based wind turbines attached to weak AC grid," in *Proc. 17th Int. Conf. Elect. Machines Syst.*, 2014, pp. 2618–2624.